

pubs.acs.org/Macromolecules Article

Coarse-Grained Molecular Dynamics Modeling of Polyvinyl Chloride: Solvent Interactions, Mechanical Behavior, and Dehydrochlorination Effects

Feranmi V. Olowookere, Gabriel D. Barbosa, and C. Heath Turner*



Cite This: Macromolecules 2023, 56, 10006-10015



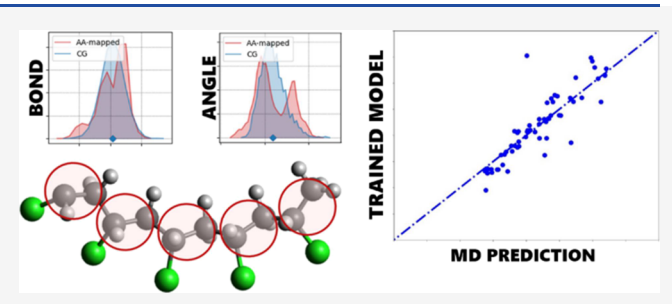
ACCESS I

III Metrics & More

Article Recommendations

Supporting Information

ABSTRACT: In this work, we develop and validate coarse-grained (CG) models for simulating the intrinsic thermophysical properties of polyvinyl chloride (PVC) and dehydrochlorinated PVC (DHPVC). The CG models are generated by using fuzzy self-tuning particle swarm optimization and iterative Boltzmann inversion, and they provide results consistent with the all-atom PVC model and with available experimental data. Several properties are evaluated within different solvents—acetone, ethyl acetate, water, and tetrahydrofuran—including bond lengths, angles, dihedral distributions, radius of gyration ($R_{\rm g}$), end-to-end



distance (R), radial distribution functions (RDFs), surface area, and potential of mean force. Additionally, CG models are validated by benchmarking mechanical properties in melt (MELT) systems, such as the stress–strain relationship and glass transition temperature. The CG model for DHPVC reliably predicts the physical changes observed after dehydrochlorination in ETA and MELT, by accurately depicting changes in dihedral distributions, polymer chain planarity, R_g , R, RDF variations, and the consequential reduction in melt viscosity. These validated CG models enable computationally efficient simulations of PVC and DHPVC interactions in various solvents and melts.

1. INTRODUCTION

The rapid accumulation of plastic waste demands innovative and sustainable recycling/upcycling strategies, and this prompts more theoretical and modeling studies of these materials. One of the more problematic plastic wastes is polyvinyl chloride (PVC), a prevalent polymer used in numerous sectors, including packaging, construction, healthcare, and electronics. 1,2 The majority of PVC waste management studies focus on dehydrochlorination (i.e., the removal of HCl) to create safer disposal products.^{3–6} This reaction occurs as the Cl atoms on the PVC backbone become susceptible to acid, base, and/or heat, giving rise to polyene segments, presenting activated sites that facilitate complete and selective depolymerization into smaller molecules. Therefore, in an effort to capitalize on the residual value of waste PVC, there is motivation to further understand the molecular characteristics of PVC before and after dehydrochlorination.

Each year, the global production of PVC is approximately 40 Mt, and this value has been increasing at a consistent 3% annual growth rate.⁶ Furthermore, over 150 Mt of PVC that have already been produced are nearing the end of their lifespan, increasing the urgency of economical and environmentally benign recycling/upcycling strategies.⁸ The upcycling of PVC (i.e., transforming these wastes into value-added products) is a more sustainable alternative to conventional waste management,^{6,9} yet there are still many fundamental

advances needed to create viable processes. Chemical recycling techniques (e.g., depolymerization), which convert plastic waste to the original monomers or oligomers, hold promise for recovering material resources. ^{10,11} Accordingly, depolymerization research has focused on cleaving vinyl polymers (e.g., PVC, PVA, PS) into their parent monomers, a process that is challenging to implement and control, due to the strength of the C–C bonds along the polymer backbone. ^{12,13} Nevertheless, chemical recycling could potentially yield valuable small organic molecules and recapture the hydrocarbon resources embedded in plastic waste.

Molecular dynamics (MD) simulations can potentially help guide the design of upcycling strategies for processing PVC waste. The growth in computational power and the development of improved simulation algorithms have greatly increased the quantitative performance of polymer simulation studies. Despite these advances, the inherent complexity of polymer systems often requires the application of multiscale simulation methodologies, ranging from quantum chemistry to

Received: October 31, 2023 Revised: November 10, 2023 Accepted: November 21, 2023 Published: December 5, 2023





atomistic and mesoscopic methods up to continuum modeling, in order to capture the broad range of length and time scales at which relevant phenomena emerge. 14,16 Coarse graining (CG) is an especially valuable technique for modeling polymer systems. 17 A CG molecular description facilitates the extension of molecular modeling to mesoscopic length and time scales, although at the cost of a loss in atomistic detail. Over the years, a wide array of CG methods have been proposed for various polymer systems, 18 and they are typically categorized as either bottom-up or top-down approaches. Bottom-up approaches [e.g., Iterative Boltzmann Inversion (IBI), force matching, Inverse Monte Carlo, and relative entropy] use information from the atomistic model to develop the CG model, while topdown approaches use experimental data for the same purpose. Notably, the Martini force field, which combines atomistic information and experimental data, has demonstrated good accuracy when compared to fully atomistic models. 19-23

To the best of our knowledge, the CG of dehydrochlorinated PVC (DHPVC) has not been previously pursued, yet such a model is critical for exploring PVC end-of-life disposal, reuse, or upcycling. Prior research, such as studies by Ghasemi et al.²³ and Wu,²⁴ primarily focused on pure PVC—melt systems; the model predictions were limited to the mechanical properties of PVC and its blends. There is a pressing need for a comprehensive CG model that addresses a broader range of PVC properties, especially in solvent environments that aid the dissolution and subsequent separation of PVC. Moreover, a better understanding of the thermophysical changes in DHPVC postreaction is crucial, which is particularly relevant to the upcycling of end-of-life PVC materials. In order to explore the thermophysical properties of these polymers, we focus on the physical changes after the dehydrochlorination process rather than the chemical reactions involved.

Supplemented by findings from Xu and colleagues, ²⁵ we acknowledge that upcycling processes typically encompass a series of chemical reactions under a range of temperatures and solvent conditions. Previous studies, ^{26–32} including experimental analyses of how different compounds, additives, and blends influence DHPVC, highlight the importance of its thermal and mechanical properties, notably in pyrolysis and the study of interfacial systems involving DHPVC. ³³ The insights obtained from this study are intended to help simulate and understand the thermophysical characteristics of PVC and DHPVC, as well as future studies of polymer blends.

Here, we use the IBI method with a fuzzy self-tuning particle swarm optimization (FST-PSO) technique³⁴ and the Martini 3 force field³⁵ to develop CG models for PVC and DHPVC, based on the simulation results from the all-atom (AA) models and validation against available experimental data. For performance benchmarking, a Gaussian process (GP) surrogate model is trained to predict σ and ε values based on the volume and $T_{\rm g}$ data of the PVC-melt system. Furthermore, we validate this model by studying its interactions with various solvents as well as its mechanical behavior. We use the DHPVC model to explore the effects of dehydrochlorination on the structural properties of PVC. This modeling approach is straightforward and computationally efficient and is capable of accurately representing a wide range of PVC properties. The subsequent sections describe the details of our methodology, including our steps to validate the model through the thermophysical properties of PVC, as well as the influence of dehydrochlorination.

2. METHODS AND MODELS

MD simulations of both AA and CG models were conducted using the Gromacs $2021.1^{36,37}$ simulation package, and VMD³⁸ was used for visualization purposes.

2.1. AA Model. The simulation systems for the AA model are comprised of a single PVC chain of 120 repeating units (denoted as PVC₁₂₀) in a cubic box containing 2,000 molecules of either water (H2O), ethyl acetate (ETA), acetone (ACE), or tetrahydrofuran (THF). Additionally, 50 PVC_{120} chains are simulated in the melt (MELT) system (see Figure S1 for simulation snapshots). PVC₁₂₀ was chosen here, as it was previously identified as a reliable model for evaluating the thermophysical properties of PVC.³⁹ To describe the bonded and nonbonded interactions, the optimized potentials for liquid simulations (OPLS) OPLS-AA⁴⁰ force field was used. This force field has been shown to accurately reproduce the experimental density of polymers³⁹ among other properties.^{41,42} The atomic charges and parameters for the polymer and solvents were obtained using PolyParGen⁴³ with the ab initio HF STO-3G method and LigParGen⁴⁴ with the 1.14*CM1A-LBCC method,⁴⁵ respectively. We refer the reader to our previous study for a detailed description of our simulation protocol and analyses of the PVC-solvent and PVC-melt systems for the AA model.³⁹

The umbrella sampling method,⁴⁶ combined with the weighted histogram analysis method⁴⁷ via *gmx wham*, is utilized for estimating the potential of mean force (PMF) from biased simulations. Here, the end-to-end distance of the PVC₁₂₀ model is defined as the reaction coordinate. A spacing of 0.1 nm between each simulation window and a spring constant of 1,000 kJ/mol m² ensures a sufficient probability distribution overlap. The same parameters and models as described earlier are maintained for the umbrella sampling simulations, with 20 ns of equilibration and 10 ns of production, providing reliable PMF estimates.

2.2. Coarse-Grained Models. The CG model for pure PVC was developed by representing one PVC repeat unit (Figure S3) with a single bead. The nonbonded parameters for the CG model were chosen from the Martini 3 force field 19 by comparing the solvation energies of one PVC repeat unit in H_2O , ETA, ACE, and THF (see Table 1), as they represent an essential part of the intermolecular

Table 1. Solvation Energy Values (kJ/mol) for a Single PVC Repeat Unit (Chloroethylene) in Various Solvents^a

bead	PVC-H ₂ O	PVC-ETA	PVC-ACE	PVC-THF
AA	1.7 (0.1)	-10.5(0.1)	-11.2 (0.1)	-10.8(0.1)
X1	7.1 (0.1)	-12.9(0.1)	-10.4 (0.1)	-14.0(0.1)
X3	3.9 (0.1)	-16.9(0.1)	-13.7(0.1)	-16.8 (0.1)
X4	1.2 (0.2)	-19.1(0.1)	-15.5(0.1)	-18.1(0.1)

""AA" and "X" annotations denote the all-atom model and the halogenated segments of PVC, respectively, with the numeric suffix on "X", indicating the interaction strength (e.g., "X4" signifies the strongest halogenated bead). 95% confidence integrals are indicated in parentheses. As a benchmark, the experimental solvation of chloroethylene in water is -2.5 ± 2.5 kJ/mol and the ATB database predicts 1.4 ± 1.4 kJ/mol. 52

interactions that drives the behavior of PVC in these solvents. The solvation energies were calculated using the multistate Bennett acceptance ratio estimator (MBAR) method. The coupling parameters for the van der Waals (vdW) and Coulombic interactions were varied between 0.00 and 1.00 ($\lambda_{\rm vdw/coul}=0.00$, 0.05, 0.10,..., 1.00), where the columbic interactions were decoupled followed by the vdW interactions, to obtain a reasonable overlap matrix using the convergence test proposed by Klimovich et al. Following an equilibration period of 1 ns, the production phase ran for 10 ns, which is sufficient for obtaining accurate free energy estimates. The Alchemical Analysis package was used to estimate the free energies using the MBAR method.

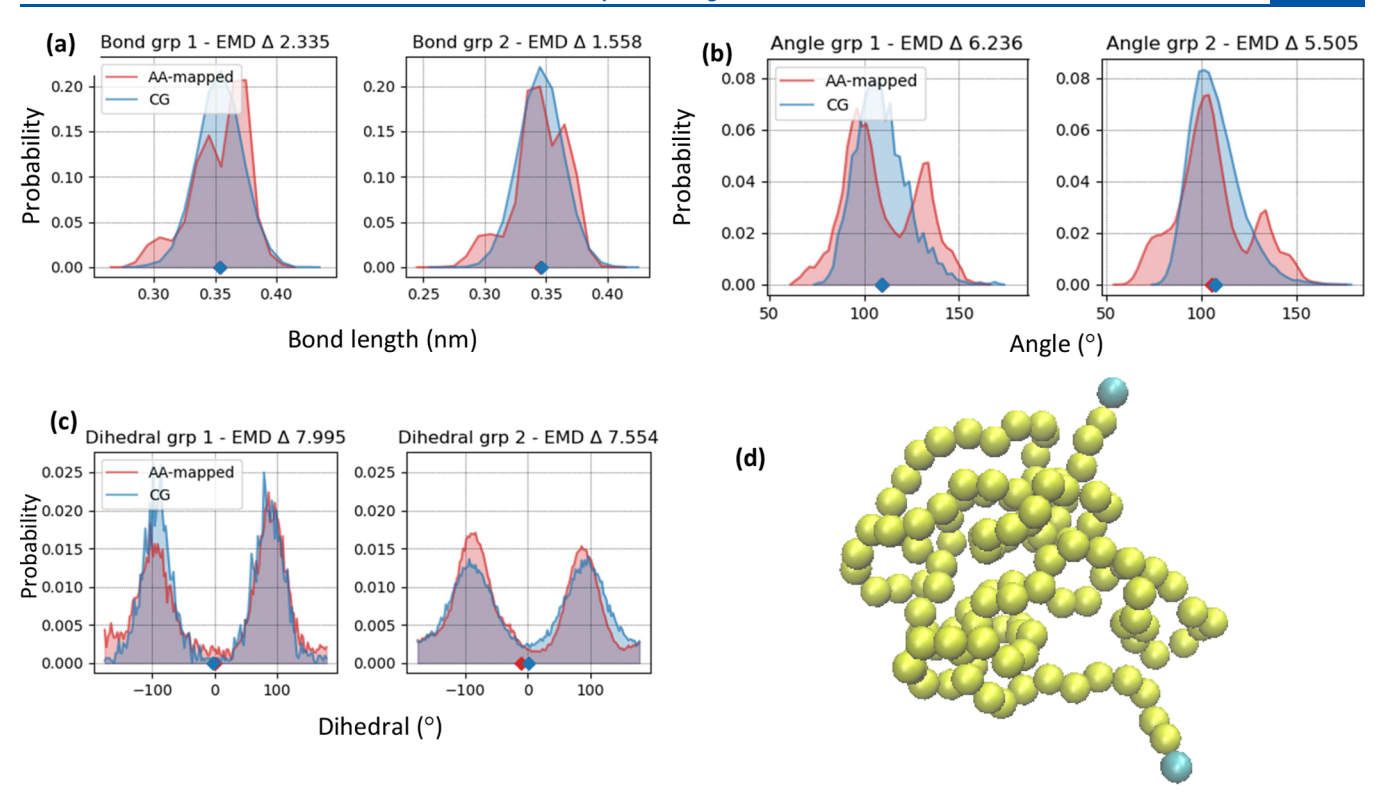


Figure 1. Structural comparisons of AA and CG PVC models: (a) bonds, (b) angles, and (c) dihedrals; (d) Bead groups—Group 1 represent the head and tail of the PVC chain, while Group 2 represents the interior beads (color code: cyan—Group 1, yellow—Group 2).

Table 2. Optimized Values for the CG Parameters^a

	equation	parameters	Group 1	Group 2
bond	$V_{\rm b} = \frac{1}{2} K_{\rm r} (r - r_{\rm o})$	$r_{\rm o}~({ m nm})$	0.29 (0.02)	0.28 (0.03)
	2 10 07	$K_{\rm r}~({\rm kJ~mol^{-1}~nm^{-4}})$	8257.9 (1925.6)	9103.7 (1190.5)
angle	$V_{\rm a} = \frac{1}{2} K_{\theta} (\cos \theta - \cos \theta_{\rm o})^2$	$ heta_{ m o}$ (°)	133.1 (1.6)	126.2 (4.1)
	a 2 0 0	K_{θ} (kJ mol ⁻¹)	117.1 (11.3)	140.7 (25.3)
dihedral	$V_{\rm d} = K_{\Phi}(1 + \cos\left(n\Phi - \Phi_{\rm s}\right))$	$\Phi_{ m s}$ (°)	2.8 (3.2)	4.1 (1.1)
		K_{Φ} (kJ mol ⁻¹)	1.8 (0.7)	1.8 (0.5)

[&]quot;Values in the parentheses represent a 95% confidence interval of CG parameters obtained from three separate optimization runs. Group 1 beads represent the head and tail of the PVC chain, while Group 2 beads represent the interior beads (see Figure 1d).

In terms of bead choice, we focused primarily on the "X" beads in the Martini 3 force field, which represent the halogenated part of the molecule, due to the presence of a chlorine atom in the PVC repeat unit. Based on the comparison of solvation energies summarized in Table 1, we chose the X3 bead for our CG model, ensuring a reasonable representation of its nonbonded interactions across different solvent environments, including both aprotic and protic types. We further confirmed our choice using a trained GP surrogate model that predicts σ and ε based on the volume and $T_{\rm g}$ of the pure PVC—melt system, as detailed in Section S1. The optimal parameters from this model agree closely with the Martini force field.³⁵

The bonded parameters of the model were initially calculated using the Boltzmann inversion method after simulating the AA model of PVC in ETA. The beads are classified into two groups: Group 1 represents the terminal beads of the PVC chain, and Group 2 represents the interior beads (see Figure 1d). This distinction captures the end effects inherent in polymer systems, where terminal units often exhibit different behaviors than interior ones due to differences in local environment and connectivity. To reproduce the bond length, angle, and dihedral distributions of the AA reference system, these parameters were then optimized using a FST-PSO technique within the Swarm CG package. This optimization process involved 112 iterations, in which a scoring function based on the earth mover's distance 4 evaluates the current bonded parameters by

comparing the resulting distributions to those of the AA-mapped reference trajectory. Here, an iteration refers to a single step of bonded parameter calculation by the swarm, while a cycle represents 50 iterations. Three optimization cycles were performed in total. The first cycle focused solely on bonds and angles, with the best parameters from this cycle being used to generate the subsequent swarm. The second cycle optimized angles and dihedrals, while the third cycle focused on optimizing the three combined geometries. Each of the first two cycles ran for 10 ns, while the third cycle lasted 25 ns. While the dihedral force constants in our model are relatively low, they remain in the same range as those in the AA model, making it essential to retain the dihedral parameters. Table 2 summarizes the bond and angle parameters of the CG model, which were obtained from the statistical average of three independent optimization runs. Additional details are provided in the topology file in the Supporting Information (Scheme S1). To validate the CG model, the simulation conditions for the AA model described earlier were also employed for performing the CG model simulations for the PVC-H₂O, PVC-ETA, PVC-ACE, PVC-THF, and PVC-MELT systems to obtain the structural and mechanical properties.

To extend our investigation, we also developed a CG model for DHPVC, which is an important derivative of PVC that exhibits distinct properties due to the presence of double bonds along the PVC backbone. In this study, the locations of these double bonds and

the accompanying chlorine atom removal were randomly selected to mimic the typical results of the chemical reactions associated with the dehydrochlorination process. The adopted the previously discussed procedure to reparametrize the CG model for 10% DHPVC (i.e., 10% of the original Cl sites have been removed on a mass basis) and then applied the derived bond, angle, and dihedral parameters to other dehydrochlorination levels investigated in this study (20 and 40%). Additionally, we recalibrated these models to ensure their alignment with the parameters derived, validating our methodology. This information is also detailed in the topology file provided in Scheme S2. This model is subsequently employed to analyze the structural, mechanical, and rheological characteristics of DHPVC in ETA and MELT with varying degrees of dehydrochlorination (10, 20, and 40%).

The Gromacs package utilities gmx rdf, gmx distance, gmx gyrate, gmx sasa, gmx angle, and gmx polystat were used to determine the radial distribution functions (RDFs), end-to-end distance (R), radius of gyration (R_g) , surface area per repeat unit (SASA/N), dihedral distribution, and mean square internal distance (MSID) per repeat unit respectively. The shape descriptors were obtained using the PLUMED package 56 and the mapped trajectory of the CG model was generated from the AA model using the gmx traj command. The RDFs were calculated on a center-of-geometry basis to evaluate the PVC—solvent and PVC—PVC interactions. By default, all simulated data correspond to T=323 K for PVC— H_2O , PVC—ETA, and PVC—THF, and T=600 K for PVC—MELT unless otherwise specified.

3. MODEL VALIDATION AND DISCUSSION

3.1. Structural and Thermodynamic Properties. To start, we compare the bond length, angle, and dihedral distributions of the CG model. As shown in Figure 1, the CG model closely aligns with these distributions with minor discrepancies. Its smoother distribution contrasts with the bimodal distribution of the AA model, which could be attributed to the unavoidable loss of some AA details intrinsic to the CG process. For instance, the repeat units along the PVC backbone of the AA model could have multiple stable configurations due to rotation around bonds, resulting in peaks at the corresponding bond lengths or angles for these states. On the other hand, the grouping of atoms into a single bead for the CG model leads to a simplification of the chain and a reduction in its degrees of freedom. As shown in Table S2, the density of the CG model is around 5% higher than that of the AA model (which is within an acceptable range as compared to other CG models developed in the literature 57-59), except for PVC-THF, where it is overestimated by 34%. This can be attributed to the inherent overestimation of the density of the Martini model for the pure THF system,⁶⁰ possibly leading to a slight overestimation of molecular packing in these systems.

The R and $R_{\rm g}$ values of the CG model shown in Figure 2 closely align with those of the AA model (refer to Figures S4 and S5 for the R and $R_{\rm g}$ distributions). When the $R/R_{\rm g}$ ratios of PVC in these systems are compared, the deviation between the AA and CG models is generally low, with an average deviation of about 12.6% (refer to Table S2). The largest deviation is observed in H_2O (36.8%), and this could be attributed to the specific behavior of PVC in this highly polar solvent. In H_2O , the nonpolar PVC tends to aggregate or form clusters due to the hydrophobic effect, a behavior that might be more prominent at the atomistic level and may not be adequately captured by the CG model. In contrast, the lowest deviation is seen in PVC–MELT (1.4%), a system consisting only of PVC chains, indicating the CG model's reliable performance when describing PVC–PVC interactions. For PVC–ETA, PVC–

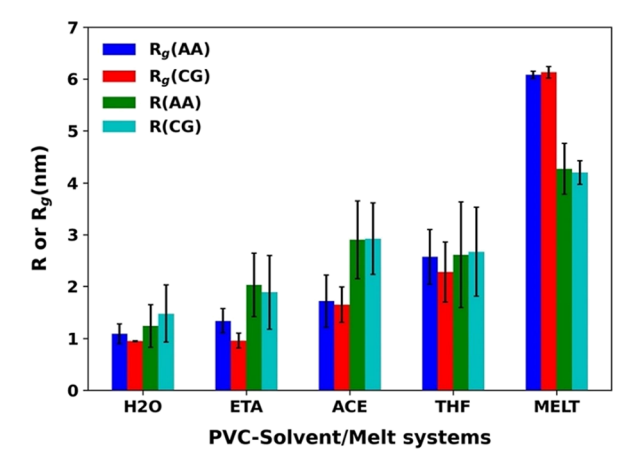


Figure 2. End-to-end distance (R), and radius of gyration (R_g) of PVC in H_2O , ETA, ACE, and THF, as well as PVC-MELT.

ACE, and PVC-THF, the deviations are much lower than in H_2O , at 6.6, 4.7, and 14.7%, respectively.

We further evaluate the intramolecular bead-bead coordination in the PVC-THF system with Figure 3a, showing a strong correlation between the CG and AA models. Similar results are found for PVC-ETA, PVC-ACE, and PVC-H₂O, as shown in Figure S6. The diminished first peak intensity in the CG model arises from the representation of grouped atoms, causing differences in short-range interactions, visible in the PMF profiles of Figure S7. This grouping results in a smoothed interaction profile compared to the AA model. Hence, differences between the PMF profiles of CG and AA at shorter distances are expected. The PVC-PVC RDF in the melt system, as depicted in Figure 3b, shows similar trends across both models. The shift of the first peak to a shorter distance (0.60 nm in the CG model compared to 0.65 nm in the AA model) could be attributed to the inherent nature of the CG model, leading to smaller interbead distances compared to interatomic distances in the AA model.

As shown in Figure 4, we investigate the RDFs between PVC and the different solvents to enhance our understanding of the respective solvent interactions. Observations from the PVC-THF and PVC-ACE systems suggest a higher degree of organization, indicating strong interactions between PVC and the solvent molecules within these systems. Minor differences in peak intensities between the CG and AA models are observed across these systems with the exception of the PVC-H₂O system. The PVC-H₂O RDF reveals a weaker interaction, consistent with the expectation of water's poor solvency for PVC. However, the CG model exhibits strong ordered peaks in water, while the AA model's RDF is more featureless. This can be attributed to the smoothing effect inherent in the CG model, which aligns water positions and intensifies the peak intensity. For comparison, additional simulations were conducted for PVC-ETA and PVC-MELT systems at T = 400 K, and similar trends were found (Figure S8 and Table S3).

Evaluation of the shape descriptors and MSID for the PVC–MELT system provided further validation of the structural properties. Shape descriptors (e.g., asphericity, acylindricity, and anisotropy) in Figure 5a present comparable values in both models. As shown in Figure 5b, we observe a consistent increase in internal distances within the polymer chain, correlating with the position of monomers along the chain.

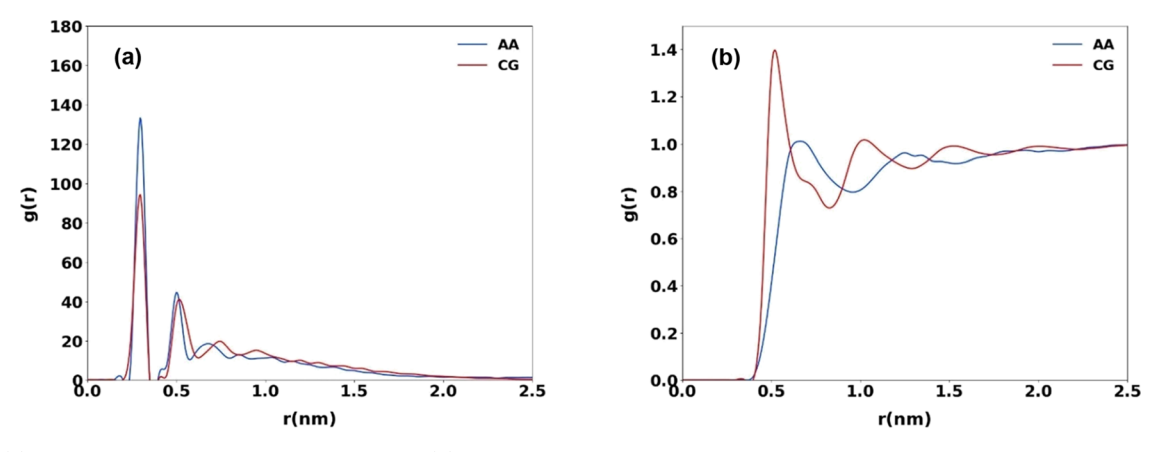


Figure 3. (a) Intramolecular RDFs of PVC in THF and (b) RDFs of PVC-PVC in the PVC-MELT system. RDFs involving the CG PVC model include both CG group types (shown in Figure 1d).

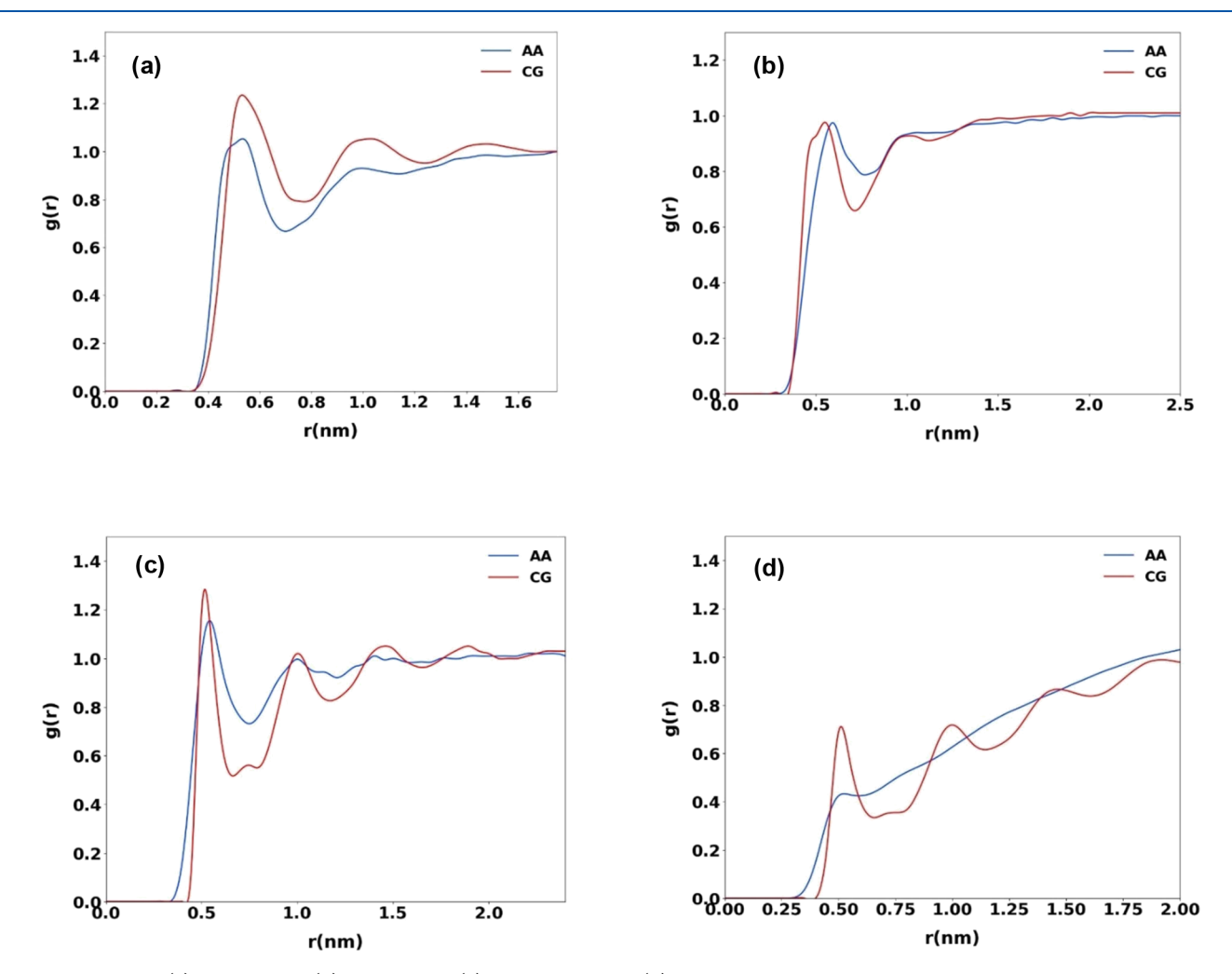


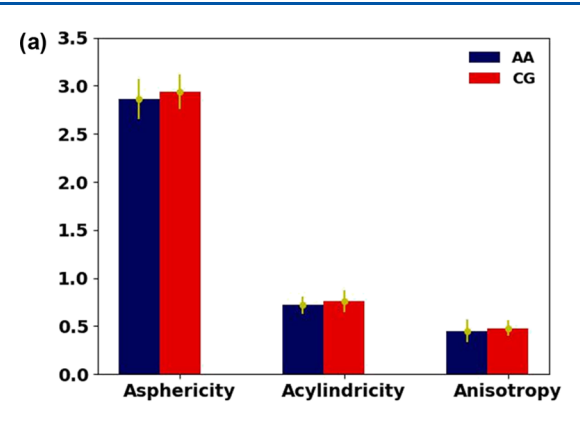
Figure 4. RDFs of (a) PVC-THF, (b) PVC-ETA, (c) PVC-ACE, and (d) PVC-H2O. All CG RDFs include both CG bead groups.

This leads to an increase in the MSID, reaching a value of up to 0.4 nm², a behavior that is characteristically exhibited by polymers.⁶¹ The CG model also effectively represents the trend of internal distances as the chain length varies, as can be seen in Figure 5b.

Table 3 provides additional evidence of the CG model performance, demonstrating its excellent agreement with the AA model in terms of the SASA/N of PVC in the PVC–MELT system when various probe sizes are used. Values of

SASA/N for the other systems can be found in Table S4. Collectively, these comparisons show the robustness of the CG model in sufficiently representing the key structural and thermodynamic aspects of the AA model.

3.2. Mechanical Properties. Following the analysis of the structural and thermodynamic properties, we examined the mechanical behavior of the models with Figure 6 showing volume—temperature plots for the CG PVC—MELT model. The identified $T_{\rm g}$ values are 366 K for AA (obtained from our



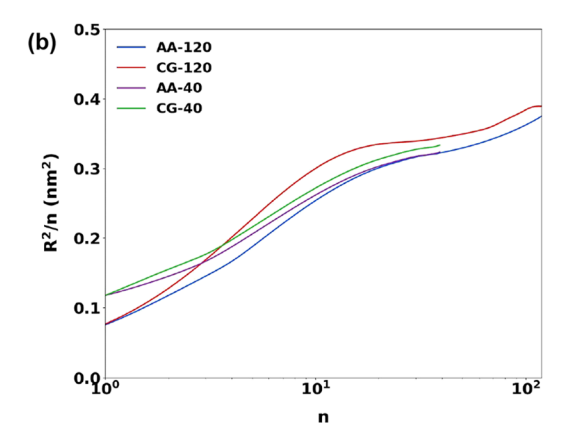


Figure 5. (a) Shape descriptors and (b) MSID of the PVC-MELT system, illustrating the ability of the CG model to represent the trend in internal distances across different chain lengths, specifically for 120 and 40 repeat units.

Table 3. SASA/N (nm²) of PVC in the PVC-MELT System^a

probe radius (nm)	AA	CG	% AA-CG deviation
0.05	0.34 (0.01)	0.33 (0.01)	2.94
0.10	0.42 (0.02)	0.41 (0.01)	2.38
0.15	0.50 (0.01)	0.48 (0.01)	4.00

^a95% confidence integrals are indicated in parentheses.

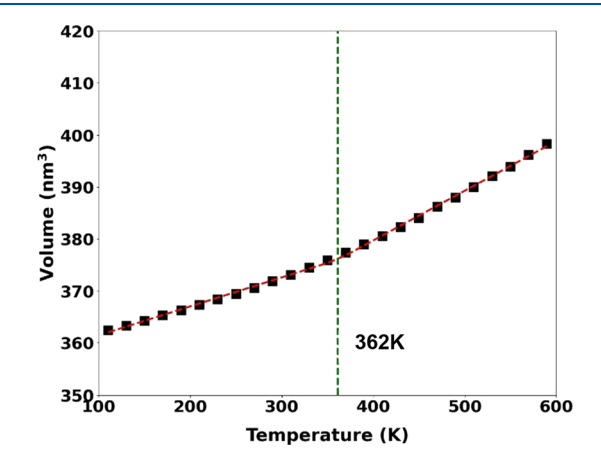


Figure 6. Simulated volume versus temperature data of the CG PVC–MELT models, along with the interpolated $T_{\rm g}$ values (green dashed line, with value indicated on the plot). The black squares are the data points and red dashed lines are fits to the data via a regularization function. ^{39,69} The experimental $T_{\rm g}$ values are reported to fall within the range of 350–370 K. ^{70–72} For comparison, the data for the AA model ($T_{\rm g}$ = 366 K) has been computed in our previous study. ³⁹

previous study³⁹) and 362 K for CG, which is consistent with experimental PVC data. $^{62-65}$ The 4 K difference in $T_{\rm g}$ might result from the coarser resolution of the CG model and its simplified depiction of thermal motions. Such differences are typical for CG models, and this deviation is smaller than some reported in the literature. 66,67 Although our simulated $T_{\rm g}$ values match the experimental range (350–370 K), exact values can vary due to the considerable difference between experimental and simulation conditions (e.g., cooling rates 68).

We further analyzed the stress-strain performance of the MELT model, as shown in Figure 7. The results agree well with experimental data at lower strain rates, with slight deviations between 2 and 5% strain rates. The close similarity

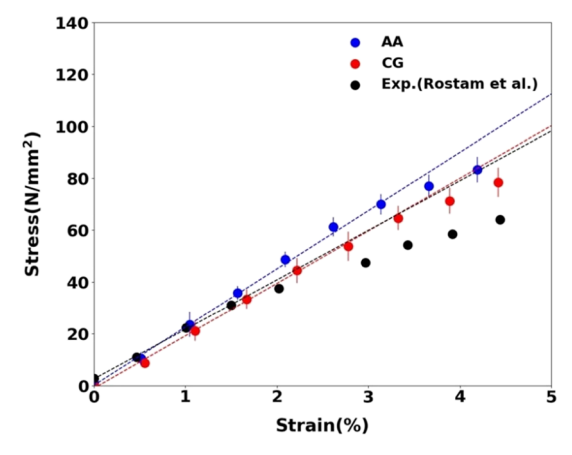


Figure 7. Stress–strain response of AA and CG PVC–MELT models at 298 K. The dashed lines represent linear fits to the elastic regions of the curves (0-2% strain rate), from which Young's modulus values are derived and presented in Table 4. Experimental values are sourced from Rostam et al. ⁷³

of the CG model (versus AA) to experimental data affirms its effectiveness. Similar Young's modulus values between the CG model and experiments in Table 4 further corroborate the model's ability to capture the mechanical properties of PVC.

Table 4. Young's Modulus of AA and CG Models in Comparison to Experimental Values⁷³

system	Young's modulus (GPa)	
exp.	2.60	
AA	2.25 (0.30)	
CG	2.03 (0.15)	

3.3. Effects of Dehydrochlorination. In this section, we evaluate the CG model's ability to capture structural changes due to varying dehydrochlorination levels. For the DHPVC–ETA system, dehydrochlorination has relatively little effect on the DHPVC's overall structure, as most metrics are within the error margins (Table S5). Yet, our RDF analysis (Figure 8) shows a decrease in the first peak of the g(r) function, indicating a proportional disruption to the DHPVC solvation shell with increased dehydrochlorination. This results in fewer solvent molecules near PVC, weakening PVC–ETA interactions. Despite some quantitative differences between AA and

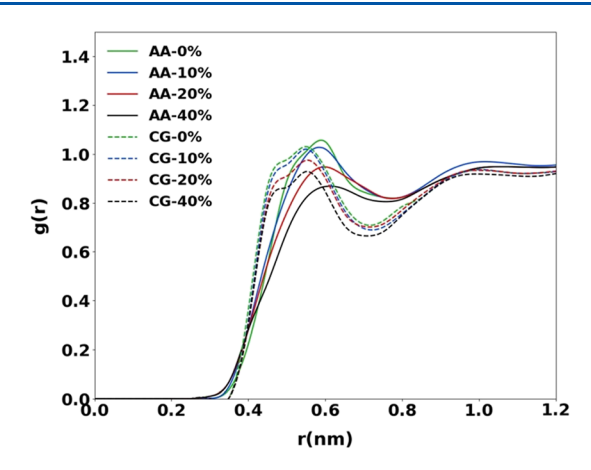


Figure 8. RDFs of DHPVC-ETA for AA and CG models corresponding to varying degrees of dehydrochlorination.

CG models, the CG model effectively captures these local deviations in these DHPVC interactions.

Figure S9 reveals dihedral distribution changes in the PVC backbone (originating from more double bonds) with an increase in 180° dihedral values and restricted dihedral motions, reflecting the more rigid DHPVC structure. These features mainly reflect local changes to the DHPVC's internal structure, and they are consistent in both AA and CG models.

For the DHPVC–MELT system, the dehydrochlorination effects are more evident. Table S6 shows decreased density with increasing dehydrochlorination, a result of reduced polymer chain mass and an expanded structure. Concurrently, there is a slight reduction in $R_{\rm g}$, suggesting a shift to a more planar polymer configuration due to increased double bonds (refer to Figure 9 for visual analysis). This aligns with observed 180° dihedral value increases in the DHPVC–ETA system (Figure S9). Additionally, the persistence length increases from 0.20 to 0.26 nm at 40% dehydrochlorination. While one might expect pronounced structural changes due to the shift toward a more planar structure, the effects are tempered. The random distribution of double bonds along the polymer chain dilutes the structural impact. This is also evident in the slight changes in the asphericity and acylindricity values.

In Figure 10, we separately analyze the RDFs of the two different types of CG beads, where the X3 beads represent the chlorinated polymer segments and the C1 beads correspond to the dehydrochlorinated segments (i.e., where double bonds have formed due to the loss of chlorine atoms). With increasing dehydrochlorination, the peak intensities in both X3–X3 and C1–C1 RDFs reduce. At 40% dehydrochlorination, similar RDF peak intensities for C1 and X3 may indicate a

balance between diminishing X3–X3 interactions and the newly formed C1–C1 interactions. As the dehydrochlorination progresses, the RDF peak gradually shifts from being dominated by X3–X3 interactions to C1–C1 interactions.

Figure 11 illustrates the relationship between the level of dehydrochlorination in DHPVC–MELT and the viscosity (obtained from $1/\eta$ versus amplitude plot in Figure S10). While experimental PVC viscosity values are typically taken below the $T_{\rm g}$, corresponding to $\sim\!60$ to 80 cP at room temperature, we cannot directly compare our data generated at 600 K. However, our values are within the same order of magnitude.

As the degree of dehydrochlorination increases, there is a notable decrease in melt viscosity, a trend that is consistent in both AA and CG models, although the decrease appears to be slightly more pronounced in the AA model. However, it is worth highlighting that despite its simplified approach, the CG model effectively captures the trend in melt viscosity (with an average deviation of 6.9%). The observed reduction in melt viscosity can be attributed to the conformational changes induced by dehydrochlorination discussed earlier; the polymer chains become more rigid, subsequently decreasing their flexibility and restricting their relative movement. Taken together, these observations highlight the influence of the dehydrochlorination level on the flow properties of DHPVC melts, which can be particularly important for industrial extrusion or injection molding processes, where the flow properties of the melt are highly impactful.

4. CONCLUSIONS

In this study, we comprehensively demonstrate the effectiveness of a new CG model, applicable to both PVC and DHPVC for predicting the thermophysical properties in different solvent environments and melt systems, as well as its consistency with available experimental data. First, we have shown that the CG model for pure PVC is capable of replicating key parameters, such as bond lengths, angle and dihedral distributions, RDF variations, shape descriptors, MSID, T_g , and stress-strain profiles, within different solvents and in the melt state. Second, the CG model for DHPVC reliably predicts the physical changes observed after dehydrochlorination in the ETA solvent and in the MELT environments by accurately depicting changes in dihedral distributions, polymer chain planarity, RDF variations, and the consequential reduction in melt viscosity. However, it is important to recognize that the dynamics of the CG models significantly deviate from the AA representation, which is an expected weakness of the CG process (see Figure S11). For a more accurate representation of the PVC dynamic properties

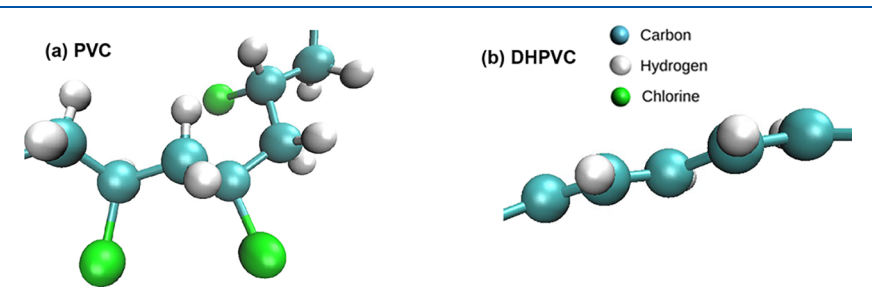
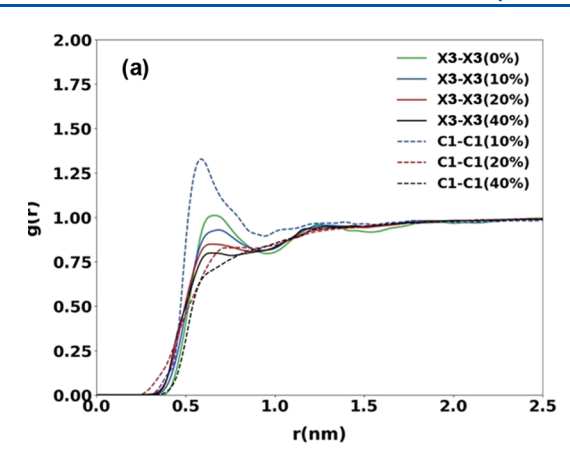


Figure 9. Comparison of molecular configurations between (a) PVC and (b) DHPVC, highlighting the more planar structure in areas near double bonds in DHPVC. See Figure S9 for the dihedral distribution, which indicates a higher occurrence of 180° dihedrals.



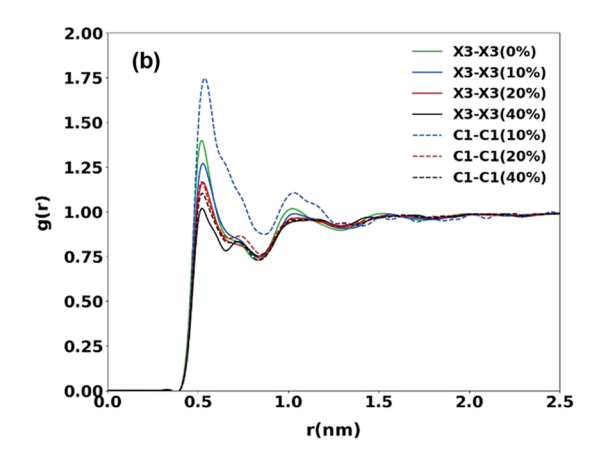


Figure 10. RDF for DHPVC-MELT for (a) AA and (b) CG models according to varying degrees of dehydrochlorination, as indicated. The "X3" beads represent the halogenated (chlorinated) groups, and the "C1" beads correspond to the dehydrochlorinated groups.

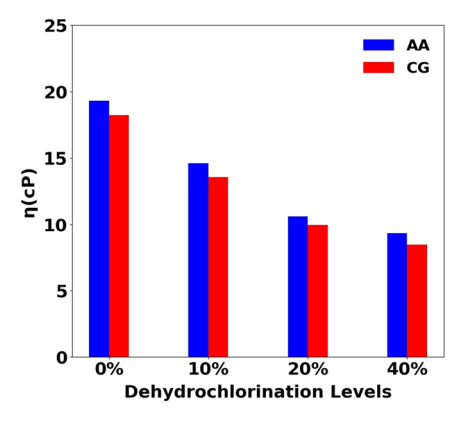


Figure 11. Viscosity (η) of 0, 10, 20, and 40% DHPVC–MELT for AA and CG models at 600 K. *Note*: the *x*-axis is not a linear scale. As a benchmark, the zero-shear viscosity of pure PVC at 298 K is 60–80 cP. ⁷⁴

when using the CG model, we suggest considering a scaling factor or correction function, as has been described in other studies. 58,76,77

ASSOCIATED CONTENT

Data Availability Statement

The data sets generated during and/or analyzed during the current study are available from the corresponding author on reasonable request.

Supporting Information

The Supporting Information is available free of charge at https://pubs.acs.org/doi/10.1021/acs.macromol.3c02211.

Additional PVC properties at different temperatures; surface area calculations using different probe sizes; shape descriptors; additional RDF analyses; angle distributions; additional mechanical properties; and molecular topologies for the simulated systems (PDF)

AUTHOR INFORMATION

Corresponding Author

C. Heath Turner — Department of Chemical and Biological Engineering, The University of Alabama, Tuscaloosa, Alabama 35487-0203, United States; oorcid.org/0000-0002-5707-9480; Phone: 205-348-1733; Email: hturner@eng.ua.edu

Authors

Feranmi V. Olowookere – Department of Chemical and Biological Engineering, The University of Alabama, Tuscaloosa, Alabama 35487-0203, United States

Gabriel D. Barbosa — Department of Chemical and Biological Engineering, The University of Alabama, Tuscaloosa, Alabama 35487-0203, United States

Complete contact information is available at: https://pubs.acs.org/10.1021/acs.macromol.3c02211

Notes

The authors declare no competing financial interest.

ACKNOWLEDGMENTS

This work is supported by the National Science Foundation EFRI E3P (Award #: 2132133). We are grateful to the Alabama Supercomputer Authority for computational support.

REFERENCES

- (1) Millet, H.; Vangheluwe, P.; Block, C.; Sevenster, A.; Garcia, L.; Antonopoulos, R. The nature of plastics and their societal usage. *Plastics and the Environment* **2018**, 2018, 1–20.
- (2) Liu, Y.; Zhou, C.; Li, F.; Liu, H.; Yang, J. Stocks and flows of polyvinyl chloride (PVC) in China: 1980–2050. Resour. Conserv. Recycl. 2020, 154, No. 104584.
- (3) Merah, N.; Bazoune, A.; Fazal, A.; Khan, Z. Weathering degradation mechanisms of chlorinated PVC. *Int. J. Plast. Technol.* **2013**, *17*, 111–122.
- (4) Sadat-Shojai, M.; Bakhshandeh, G.-R. Recycling of PVC wastes. *Polymer Degradation and Stability* **2011**, *96* (4), 404–415.
- (5) Glas, D.; Hulsbosch, J.; Dubois, P.; Binnemans, K.; De Vos, D. E. End-of-Life Treatment of Poly (Vinyl Chloride) and Chlorinated Polyethylene by Dehydrochlorination in Ionic Liquids. *ChemSusChem* **2014**, 7 (2), 610–617.
- (6) Oster, K.; Tedstone, A.; Greer, A. J.; Budgen, N.; Garforth, A.; Hardacre, C. Dehydrochlorination of PVC in multi-layered blisterpacks using ionic liquids. *Green Chem.* **2020**, 22 (15), 5132–5142.
- (7) Park, E. J.; Lee, S. Y.; Canlier, A.; Hwang, T. S. Controlled dehydrochlorination of poly (vinyl chloride) for fabrication of membranes with polyacetylene-like structure: XPS analysis and ion exchange membrane discussion. *Macromol. Res.* **2019**, *27*, 33–47.
- (8) Brown, K.; Holland, M.; Boyd, R.; Thresh, S.; Jones, H.; Ogilvie, S. Economic Evaluation of PVC Waste Management-A report produced for European Commission Environment Directorate. Retrieved September, 2000; Vol. 24, p. 2007.

- (9) Balu, R.; Dutta, N. K.; Roy Choudhury, N. Plastic Waste Upcycling: A Sustainable Solution for Waste Management, Product Development, and Circular Economy. *Polymers* **2022**, *14* (22), 4788.
- (10) Rahimi, A.; García, J. M. Chemical recycling of waste plastics for new materials production. *Nat. Rev. Chem.* **2017**, *1* (6), No. 0046.
- (11) Achilias, D.; Roupakias, C.; Megalokonomos, P.; Lappas, A.; Antonakou, E. Chemical recycling of plastic wastes made from polyethylene (LDPE and HDPE) and polypropylene (PP). *J. Hazard. Mater.* **2007**, 149 (3), 536–542.
- (12) Iyim, T.; Güclü, G.; Emik, S.; Kilinç, S.; Özgümüş, S. Mechanical and migration properties of PVC/waste PET depolymerization products blends. *J. Macromol. Sci. A* **2005**, 42 (6), 801–810.
- (13) Tomar, P. A.; Yadav, S.; Gupta, G. R. The thermal gravimetric studies for polymer samples of polyvinyl chloride (PVC) and polyvinyl alcohol (PVA) obtained by treatment with ionic liquid [bmim] Br. *Polym. Bull.* **2014**, *71*, 1349–1358.
- (14) Gooneie, A.; Schuschnigg, S.; Holzer, C. A review of multiscale computational methods in polymeric materials. *Polymers* **2017**, *9* (1), 16.
- (15) Li, Y.; Abberton, B. C.; Kröger, M.; Liu, W. K. Challenges in multiscale modeling of polymer dynamics. *Polymers* **2013**, *5* (2), 751–832.
- (16) Ricci, E.; Vergadou, N. Integrating Machine Learning in the Coarse-Grained Molecular Simulation of Polymers. *J. Phys. Chem. B* **2023**, *127* (11), 2302–2322.
- (17) Joshi, S. Y.; Deshmukh, S. A. A review of advancements in coarse-grained molecular dynamics simulations. *Mol. Sim.* **2021**, 47 (10–11), 786–803.
- (18) Dhamankar, S.; Webb, M. A. Chemically specific coarse-graining of polymers: Methods and prospects. *J. Polym. Sci.* **2021**, 59 (22), 2613–2643.
- (19) Marrink, S. J.; Risselada, H. J.; Yefimov, S.; Tieleman, D. P.; De Vries, A. H. The MARTINI force field: coarse grained model for biomolecular simulations. *J. Phys. Chem. B* **2007**, *111* (27), 7812–7824
- (20) Barbosa, G. D.; Turner, C. H. Martini Coarse-Grained Model for Poly(alkylimidazolium) Ionenes and Applications in Aromatic Compound Extraction. *Macromolecules* **2022**, *55* (1), 26–34.
- (21) Rossi, G.; Monticelli, L.; Puisto, S. R.; Vattulainen, I.; Ala-Nissila, T. Coarse-graining polymers with the MARTINI force-field: polystyrene as a benchmark case. *Soft Matter* **2011**, *7* (2), 698–708.
- (22) Brosz, M.; Michelarakis, N.; Bunz, U. H.; Aponte-Santamaría, C.; Gräter, F. Martini 3 coarse-grained force field for poly (paraphenylene ethynylene) s. *Phys. Chem. Chem. Phys.* **2022**, 24 (17), 9998–10010.
- (23) Ghasemi, H.; Yazdani, H. Plastics and sustainability in the same breath: Machine learning-assisted optimization of coarse-grained models for polyvinyl chloride as a common polymer in the built environment. *Resour. Conserv. Recycl.* **2022**, *186*, No. 106510.
- (24) Wu, C. Coarse-grained molecular dynamics simulations of stereoregular poly(methyl methacrylate)/poly(vinyl chloride) blends. *J. Polym. Sci. B Polym. Phys.* **2015**, *53* (3), 203–212.
- (25) Xu, S.; Han, Z.; Yuan, K.; Qin, P.; Zhao, W.; Lin, T.; Zhou, T.; Huang, F. Upcycling chlorinated waste plastics. *Nat. Rev. Methods Primers* **2023**, 3 (1), 44.
- (26) Ahmad, N.; Kausar, A.; Muhammad, B. Perspectives on polyvinyl chloride and carbon nanofiller composite: a review. *Polym.-Plast. Technol. Eng.* **2016**, *55*, 1076–1098.
- (27) Bowley, H.; Gerrard, D.; Biggin, I. The effect of amines on the dehydrochlorination of poly (vinyl chloride). *J. Vinyl Technol.* **1988**, 10, 50–52.
- (28) Turhan, Y.; Dogan, M.; Alkan, M. Poly (vinyl chloride)/kaolinite nanocomposites: characterization and thermal and optical properties. *Ind. Eng. Chem. Res.* **2010**, *49*, 1503–1513.
- (29) Abdel-Naby, A. S.; El Hefnawy, M. Improvement of the thermal and mechanical properties of poly (vinyl chloride) in presence of poly (ethylene succinate). *Polym. Test.* **2003**, 22, 25–29.

- (30) Mukherjee, A.; Gupta, A. Dehydrochlorination of Poly (vinyl Chloride) in Pyridine. III. Thermal and Mechanical Properties. *J. Macromol. Chem.* **1981**, *16*, 1323–1333.
- (31) Benaniba, M. T.; Massardier-Nageotte, V. Evaluation effects of biobased plasticizer on the thermal, mechanical, dynamical mechanical properties, and permanence of plasticized PVC. *J. Appl. Polym. Sci.* **2010**, *118*, 3499–3508.
- (32) Moulay, S. Chemical modification of poly (vinyl chloride)—Still on the run. *Prog. Polym. Sci.* **2010**, *35*, 303–331.
- (33) Li, S.; Aphale, S. S.; Budzinski, K.; DesJardin, P. E.; Swensen, D. Modeling the response of blended PVC/PET fabrics to fire environments. *Fire Saf. J.* **2022**, *129*, No. 103557.
- (34) Empereur-Mot, C.; Pesce, L.; Doni, G.; Bochicchio, D.; Capelli, R.; Perego, C.; Pavan, G. M. Swarm-CG: automatic parametrization of bonded terms in MARTINI-based coarse-grained models of simple to complex molecules via fuzzy self-tuning particle swarm optimization. *ACS omega* **2020**, *5* (50), 32823–32843.
- (35) Souza, P. C.; Alessandri, R.; Barnoud, J.; Thallmair, S.; Faustino, I.; Grünewald, F.; Patmanidis, I.; Abdizadeh, H.; Bruininks, B. M.; Wassenaar, T. A. Martini 3: a general purpose force field for coarse-grained molecular dynamics. *Nat. Methods* **2021**, *18* (4), 382–388
- (36) Abraham, M. J.; Murtola, T.; Schulz, R.; Páll, S.; Smith, J. C.; Hess, B.; Lindahl, E. GROMACS: High performance molecular simulations through multi-level parallelism from laptops to supercomputers. *SoftwareX* **2015**, *1*, 19–25.
- (37) Kutzner, C.; Kniep, C.; Cherian, A.; Nordstrom, L.; Grubmüller, H.; de Groot, B. L.; Gapsys, V. GROMACS in the cloud: A global supercomputer to speed up alchemical drug design. *J. Chem. Inf. Model.* **2022**, *62* (7), 1691–1711.
- (38) Humphrey, W.; Dalke, A.; Schulten, K. VMD: visual molecular dynamics. *J. Mol. Graphics* **1996**, *14* (1), 33–38.
- (39) Olowookere, F. V.; Al Alshaikh, A.; Bara, J. E.; Turner, C. H. Effects of chain length on the structure and dynamics of polyvinyl chloride during atomistic molecular dynamics simulations. *Mol. Simul.* **2023**, *15*, 1401–1412.
- (40) Jorgensen, W. L.; Maxwell, D. S.; Tirado-Rives, J. Development and testing of the OPLS all-atom force field on conformational energetics and properties of organic liquids. *J. Am. Chem. Soc.* **1996**, 118 (45), 11225–11236.
- (41) Odegard, G.; Clancy, T.; Gates, T. Prediction of mechanical properties of polymers with various force fields. In 46th AIAA/ASME/ASCE/AHS/ASC Structures, Structural Dynamics and Materials Conference, 2005, p. 1850.
- (42) Fang, C.-E.; Tsai, Y.-C.; Scheurer, C.; Chiu, C.-C. Revised atomic charges for OPLS force field model of poly (ethylene oxide): Benchmarks and applications in polymer electrolyte. *Polymers* **2021**, 13 (7), 1131.
- (43) Yabe, M.; Mori, K.; Ueda, K.; Takeda, M. Development of PolyParGen Software to facilitate the determination of molecular dynamics simulation parameters for polymers. *J. Comput. Chem., Jpn.* **2019**, *5*, No. 2018-0034.
- (44) Dodda, L. S.; Cabeza de Vaca, I.; Tirado-Rives, J.; Jorgensen, W. L. LigParGen web server: an automatic OPLS-AA parameter generator for organic ligands. *Nucleic acids research* **2017**, *45* (W1), W331–W336.
- (45) Dodda, L. S.; Vilseck, J. Z.; Tirado-Rives, J.; Jorgensen, W. L. 1.14* CM1A-LBCC: localized bond-charge corrected CM1A charges for condensed-phase simulations. *J. Phys. Chem. B* **2017**, *121* (15), 3864–3870.
- (46) Torrie, G. M.; Valleau, J. P. Nonphysical sampling distributions in Monte Carlo free-energy estimation: Umbrella sampling. *J. Comput. Phys.* **1977**, 23 (2), 187–199.
- (47) Kumar, S.; Rosenberg, J. M.; Bouzida, D.; Swendsen, R. H.; Kollman, P. A. The weighted histogram analysis method for free-energy calculations on biomolecules. *I. The method. J. Comput. Chem.* **1992**, *13* (8), 1011–1021.

- (48) Shirts, M. R.; Chodera, J. D. Statistically optimal analysis of samples from multiple equilibrium states. *J. Chem. Phys.* **2008**, *129* (12), 124105.
- (49) Shirts, M. R.; Pitera, J. W.; Swope, W. C.; Pande, V. S. Extremely precise free energy calculations of amino acid side chain analogs: Comparison of common molecular mechanics force fields for proteins. *J. Chem. Phys.* **2003**, *119* (11), 5740–5761.
- (50) Klimovich, P. V.; Shirts, M. R.; Mobley, D. L. Guidelines for the analysis of free energy calculations. *J. Comput. Aided Mol. Des.* **2015**, 29, 397–411.
- (51) Saravi, S. H.; Panagiotopoulos, A. Z. Individual ion activity coefficients in aqueous electrolytes from explicit-water molecular dynamics simulations. *J. Phys. Chem. B* **2021**, *125* (30), 8511–8521.
- (52) Malde, A. K.; Zuo, L.; Breeze, M.; Stroet, M.; Poger, D.; Nair, P. C.; Oostenbrink, C.; Mark, A. E. An automated force field topology builder (ATB) and repository: version 1.0. *J. Chem. Theory Comput.* **2011**, *7* (12), 4026–4037.
- (53) Yagyu, H.; Utsumi, T. Coarse-grained molecular dynamics simulation of nanofilled crosslinked rubber. *Comput. Mater. Sci.* **2009**, 46 (2), 286–292.
- (54) Pele, O.; Werman, M. Fast and robust Earth Mover's Distances. In 2009 IEEE 12th International Conference on Computer Vision, 2009, pp. 460-467.
- (55) Baum, B.; Wartman, L. H. Structure and mechanism of dehydrochlorination of polyvinyl chloride. *J. Polym. Sci.* **1958**, 28 (118), 537–546.
- (56) Tribello, G. A.; Bonomi, M.; Branduardi, D.; Camilloni, C.; Bussi, G. PLUMED 2: New feathers for an old bird. *Comput. Phys. Commun.* **2014**, *185* (2), 604–613.
- (57) Luz, A. M.; Barbosa, G.; Manske, C.; Tavares, F. W. Tween-80 on Water/Oil Interface: Structure and Interfacial Tension by Molecular Dynamics Simulations. *Langmuir* **2023**, 39 (9), 3255–3265.
- (58) Peters, B. L.; Salerno, K. M.; Agrawal, A.; Perahia, D.; Grest, G. S. Coarse-Grained Modeling of Polyethylene Melts: Effect on Dynamics. *J. Chem. Theory Comput.* **2017**, *13* (6), 2890–2896.
- (59) Fritz, D.; Harmandaris, V. A.; Kremer, K.; van der Vegt, N. F. A. Coarse-Grained Polymer Melts Based on Isolated Atomistic Chains: Simulation of Polystyrene of Different Tacticities. *Macromolecules* **2009**, 42 (19), 7579–7588.
- (60) Alessandri, R.; Barnoud, J.; Gertsen, A. S.; Patmanidis, I.; de Vries, A. H.; Souza, P. C.; Marrink, S. J. Martini 3 coarse-grained force field: small molecules. *Adv. Theory Simul.* **2022**, *5* (1), No. 2100391.
- (61) Perez, M.; Lame, O.; Leonforte, F.; Barrat, J.-L. Polymer chain generation for coarse-grained models using radical-like polymerization. *J. Chem. Phys.* **2008**, *128* (23), 234904.
- (62) Lindström, A.; Hakkarainen, M. Environmentally friendly plasticizers for poly (vinyl chloride)—Improved mechanical properties and compatibility by using branched poly (butylene adipate) as a polymeric plasticizer. J. Appl. Polym. Sci. 2006, 100 (3), 2180–2188.
- (63) Rohling, J.; Medina, A.; Pereira, J.; Rubira, A.; Bento, A.; Miranda, L.; Baesso, M. Thermal lens versus DSC measurements for glass transition analysis of polymer. *Anal. Sci./Suppl.* **2002**, *17*, s103—s105.
- (64) Ziska, J.; Barlow, J.; Paul, D. Miscibility in PVC-polyester blends. *Polymer* 1981, 22 (7), 918–923.
- (65) Da Silva, M. A.; Vieira, M. G. A.; Maçumoto, A. C. G.; Beppu, M. M. Polyvinylchloride (PVC) and natural rubber films plasticized with a natural polymeric plasticizer obtained through polyesterification of rice fatty acid. *Polym. Test.* **2011**, *30* (5), 478–484.
- (66) Hsu, D. D.; Xia, W.; Arturo, S. G.; Keten, S. Thermomechanically Consistent and Temperature Transferable Coarse-Graining of Atactic Polystyrene. *Macromolecules* **2015**, *48* (9), 3057–3068.
- (67) Tomaszewska, J.; Sterzyński, T.; Woźniak-Braszak, A.; Banaszak, M. Review of recent developments of glass transition in PVC nanocomposites. *Polymers* **2021**, *13* (24), 4336.
- (68) Mohammadi, M.; Davoodi, J. The glass transition temperature of PMMA: A molecular dynamics study and comparison of various determination methods. *Eur. Polym. J.* **2017**, *91*, 121–133.

- (69) Santos, M.; Tavares, F.; Biscaia, E., Jr Molecular thermodynamics of micellization: micelle size distributions and geometry transitions. *Braz. J. Chem. Eng.* **2016**, *33*, 515–523.
- (70) Amorim, F. C.; Souza, J. F. B.; da Costa Mattos, H. S.; Reis, J. M. L. Temperature effect on the tensile properties of unplasticized polyvinyl chloride. *SPE Polymers* **2022**, *3* (2), 99–104.
- (71) Tomaszewska, J.; Sterzyński, T.; Woźniak-Braszak, A.; Banaszak, M. Review of Recent Developments of Glass Transition in PVC Nanocomposites. *Polymers (Basel)* **2021**, *13* (24), 4336.
- (72) Takeoka, Y. Poly(vinyl chloride) (PVC). In *Encyclopedia of Polymeric Nanomaterials*, Kobayashi, S.; Müllen, K., Ed.; Springer: Berlin Heidelberg: Berlin, Heidelberg, 2015, pp. 1739–1741.
- (73) Rostam, S.; Ali, A. K.; AbdalMuhammad, F. H. Experimental investigation of mechanical properties of PVC polymer under different heating and cooling conditions. *J. Eng.* **2016**, *2016*, *1*–5.
- (74) Laine, C.; Cassagnau, P. Prediction of zero shear viscosity of poly (vinyl chloride) plastisols. *Appl. Rheol.* **2006**, *16* (3), 136–144.
- (75) Hieber, C. A. Melt-viscosity characterization and its application to injection molding. In *Injection and Compression Molding Fundamentals*; Routledge, 2017, pp. 124-129.
- (76) Agrawal, V.; Holzworth, K.; Nantasetphong, W.; Amirkhizi, A. V.; Oswald, J.; Nemat-Nasser, S. Prediction of viscoelastic properties with coarse-grained molecular dynamics and experimental validation for a benchmark polyurea system. *J. Polym. Sci. B Polym. Phys.* **2016**, 54 (8), 797–810.
- (77) Grest, G. S.; Michael Salerno, K.; Peters, B. L.; Ge, T.; Perahia, D. Resolving properties of entangled polymers melts through atomistic derived coarse-grained models. *Handbook of Materials Modeling: Methods: Theory and Modeling* **2020**, 1397–1410.